Food Control 180 (2026) 111676

Contents lists available at ScienceDirect

Food Control

journal homepage: www.elsevier.com/locate/foodcont

Visible-near infrared spectroscopy and near-infrared hyperspectral imaging for the detection of T-2 and HT-2 toxins in individual oat grains

Irene Teixido-Orries [a], Francisco Molino [a], Pau Agusti-Fernandez [b], Ebenezer Ayibiowu [c], Derek Croucher [d], Angel Medina [c], Sonia Marín [a], Carol Verheecke-Vaessen [c,*]

[a] Applied Mycology Unit, Department of Food Technology, Engineering and Science, University of Lleida, AGROTECNIO-CERCA Centre, Av. Rovira Roure 191, 25198, Lleida, Spain
[b] IRTA, Postharvest, Fruitcentre, Catalonia, 25003, Lleida, Spain
[c] Magan Centre of Applied Mycology, Cranfield University, Cranfield, MK43 0AL, United Kingdom
[d] Morning Foods, Morning Foods Limited, North Western Mills, Gresty Road, Crewe, Cheshire, CW2 6HP, United Kingdom

ARTICLE INFO

Keywords:
Applied mycology
T-2 toxin
HT-2 toxin
Near-infrared
Vis range
Spectroscopy
Oat
Cereal sorting

ABSTRACT

Oat grains are increasingly consumed worldwide due to their health benefits, yet they are highly susceptible to contamination by *Fusarium* toxins, particularly T-2 and HT-2 toxins (T-2+HT-2). These toxins pose serious health risks and are unevenly distributed, with a few highly contaminated grains often driving a batch over legal safety limits. Current detection methods are destructive, slow, or inadequate for detecting contamination at the individual grain level. This study is the first to demonstrate the potential of visible–near-infrared (Vis-NIR) spectroscopy and near-infrared hyperspectral imaging (NIR-HSI) to detect T-2+HT-2 in individual oat grains non-destructively. 200 grains were scanned, and their toxin content quantified by liquid chromatography-tandem mass spectrometry (LC-MS/MS). Classification models were developed to identify grains exceeding both the European Union (EU) legal threshold (1250 μg/kg) and a higher risk level (10,000 μg/kg). Both techniques achieved high accuracy (up to 94.5 %) in identifying contaminated grains. Key wavelengths were identified (e.g., 1203, 1419, 1424 and 1476 nm in NIR; 440–455 nm in Vis), and reducing the model to 20 wavelengths preserved performance while simplifying computation. Critically, removing just 21.5 % of the most contaminated grains could reduce overall toxin levels by over 95 %. Moreover, sampling simulations revealed that analysing 30 % of grains guarantees detection of contamination above legal limits, whereas 0.5 % sampling yields only a 25–33 % detection chance. These findings highlight a feasible path for integrating spectroscopic screening into industrial oat sorting lines, improving food safety, reducing economic losses, and overcoming key limitations of conventional mycotoxin monitoring.

1. Introduction

Oats (*Avena sativa* L.) have become an increasingly important cereal crop due to their health benefits, particularly in reducing the risk of coronary heart diseases (Thies et al., 2014), and their growing incorporation into human diets (Rasane et al., 2015). For example, corresponding with increased oat consumption trends, oat production in the United Kingdom reached 986 thousand tonnes in 2024, representing a 19 % increase compared to the previous year (DEFRA, 2024). However, oats, like other small grain cereal crops such as wheat and barley, are prone to contamination by *Fusarium* species, which can infect the crop. In oats, such infections lead to the accumulation of mycotoxins such as T-2 and HT-2 toxins (T-2+HT-2), which pose significant health risks to both humans and animals (Imathiu et al., 2017; Schuhmacher-Wolz et al., 2017). These toxins can cause damage in multiple organs, including the cardiovascular and nervous systems, as well as the gastrointestinal tract (Janik et al., 2021). Countries in Northern Europe, including the United Kingdom, are particularly affected by elevated levels of T-2+HT-2 contamination in oats, attributed mainly to the presence of *Fusarium langsethiae* (De Colli et al., 2021; Gil-Serna et al., 2022; Luo et al., 2021). *F. langsethiae* tends to colonise oat tissues without causing visible disease symptoms, making it particularly challenging to detect in the field and contributing to unnoticed accumulation of T-2+HT-2 during grain development (Isidro-Sánchez et al., 2020). To mitigate the associated health risks, the European Commission has

* Corresponding author.
E-mail address: c.verheecke@cranfield.ac.uk (C. Verheecke-Vaessen).

https://doi.org/10.1016/j.foodcont.2025.111676
Received 15 June 2025; Received in revised form 31 July 2025; Accepted 25 August 2025
Available online 26 August 2025

Nomenclature

AUC	Area under the receiver operating characteristic curve
CA	Classification accuracy
DON	Deoxynivalenol
ESI	Electrospray ionisation
ELISA	Enzyme-linked immunosorbent assay
EU	European Union
HPLC	High-performance liquid chromatography
HSI	Hyperspectral imaging
LC-MS/MS	Liquid chromatography-tandem mass spectrometry
LDA	Linear discriminant analysis
LFD	Lateral flow devices
LOD	Limit of detection
LOQ	Limit of quantification
MRM	Multiple reaction monitoring
MS	Mass spectrometry
NIR	Near-infrared
SMOTE	Synthetic minority over-sampling technique
SNV	Standard normal variate
T-2+HT-2	T-2 and HT-2 toxins
Vis	Visible range

recently updated regulatory limits for these toxins (European Commission, 2011, 2024). For unprocessed oat grains with inedible husk, a maximum permitted level has been set at 1250 μg/kg, while significantly lower thresholds apply to processed oat products destined for human consumption.

At the point of intake in the food industry, T-2+HT-2 contamination in oat batch samples is analysed before the product enters the food chain. Commonly used analytical techniques include high-performance liquid chromatography (HPLC), liquid chromatography-tandem mass spectrometry (LC-MS/MS), lateral flow devices (LFD), and enzyme-linked immunosorbent assays (ELISA). However, these conventional methods present several limitations, such as high operational costs, lengthy processing times, and limited suitability for routine screening in industrial environments (Krska et al., 2014). In some cases, their accuracy can also be insufficient. For example, preliminary results have indicated that LFD kits may yield error rates of up to 84.3 % when used to detect T-2+HT-2 in oats (article in preparation). European regulations on official controls aim to ensure scientific rigour in sampling and analysis, while acknowledging the highly heterogeneous distribution of mycotoxins in cereal batches (European Commission, 2023, pp. 1–44). Research indicates that although many oat grains are toxin-free, a small proportion of highly contaminated grains can disproportionately elevate the overall toxin levels (Blackshaw-Crosby, 2021; Teixido-Orries, Molino, Castro-Criado et al., 2025). Consequently, early identification and removal of these outlier grains could reduce toxin transfer into the food chain, improving both product safety and quality of oat-based products (Dropa et al., 2021; Teixido-Orries, Molino, Pascari, et al., 2025; Tittlemier et al., 2020).

In recent years, spectroscopic techniques such as visible and near-infrared (Vis-NIR) and NIR-hyperspectral imaging (NIR-HSI) have attracted interest for their potential to detect mycotoxins in cereals (Femenias et al., 2020). These methods are rapid, non-destructive, and require minimal sample preparation, making them suitable for real-time monitoring and automatic grain sorting in industrial settings (Fox & Manley, 2014; Zareef et al., 2021). However, their application at scale faces challenges related to model complexity and processing time. A common strategy to address this is to reduce the number of wavelengths used in classification models, thereby lowering data dimensionality, accelerating computation, and enabling real-time operation. Selecting relevant wavelengths can also provide insight into the spectral characteristics associated with mycotoxin contamination (Wan et al., 2020). Both Vis-NIR and NIR-HSI provide information on the physical and chemical properties of grains. These techniques have demonstrated potential for detecting mycotoxins such as deoxynivalenol (DON) and T-2+HT-2 in oat samples (Teixido-Orries, Molino, Femenias, et al., 2023; Teixido-Orries, Molino, Gatius, et al., 2023; Tekle et al., 2013), but their application to individual, unprocessed oat grains has not been thoroughly explored yet. If proven effective, selectively removing the most contaminated grains using spectroscopy could substantially lower the overall T-2+HT-2 levels in oat batches. Since these toxins are unevenly distributed, a small number of grains can determine whether a batch exceeds legal limits. As a result, depending on the grains selected for sampling, there is a risk of accepting contaminated batches or rejecting safe ones. Removing the most contaminated grains could help maintain lower toxin levels in accepted batches and enhance food safety and regulatory compliance (Brodal et al., 2020). Therefore, it could support more efficient and sustainable oat production by reducing food waste and minimising financial risks associated with batch rejection.

The primary objective of this study is to evaluate the effectiveness of Vis-NIR and NIR-HSI spectroscopy for detecting highly T-2+HT-2 contaminated oat grains, using LC-MS/MS as the reference method. In particular, the study aims to develop classification models that can identify grains exceeding the regulatory threshold of 1250 μg/kg, as well as an elevated threshold of 10,000 μg/kg. It also aims to simplify model complexity by selecting the 20 most relevant wavelengths. Additionally, this study examines the distribution of contamination within oat-contaminated batch samples, analyses the spectral characteristics associated with different contamination levels, and explores how this contamination impacts sampling.

2. Materials and methods

2.1. Oat samples and mycotoxin quantification

2.1.1. Oat samples

Two samples of white unprocessed oat grains (*Avena sativa* L.) were selected based on their high T-2+HT-2 content. These were collected in South Scotland and North Scotland (United Kingdom) in 2022. Sample 1 (South Scotland) had 1900 μg/kg of T-2 and 1500 μg/kg of HT-2 toxin, with a total content of 3400 μg/kg. Sample 2 (North Scotland) had 920 μg/kg of T-2 and 2200 μg/kg of HT-2 toxin, with a total content of 3120 μg/kg. From each sample, 100 individual grains were randomly selected, resulting in a total of 200 oat grains analysed in this study. While the bulk samples showed average T-2+HT-2 concentrations of 3400 μg/kg and 3120 μg/kg, individual grain analysis later revealed a highly uneven distribution, with some grains containing much higher toxin levels. This variability is further detailed in Section 3.2.

2.1.2. Chemicals and reagents

T-2 (100 μg/mL) and HT-2 toxin (100 μg/mL) standards were supplied by Romer Lab (Tulln, Austria) and were dissolved in acetonitrile. Ultrapure water was obtained with PURELAB® Chorus 1 (ELGA LabWater; Buckinghamshire, UK). Ammonium acetate (>99 %, analytical reagent grade), acetic acid glacial (99.7 %, HPLC grade), acetonitrile (LC-MS grade), and methanol (LC-MS grade) were obtained from Fisher Scientific (Waltham, MA, USA).

2.1.3. Sample preparation

T-2+HT-2 were extracted from 200 oat grains, 100 from each sample set. Oat grains were ground using the Precellys® homogeniser (Bertin Technologies, Yvelines, France). Each oat grain was incorporated in an Eppendorf tube with one 7 mm stainless steel bead and milled at a speed of 5200 rpm for 2 cycles of 10 s with a 5-s pause in between. Subsequently, 260 μL of extraction solvent, consisting of acetonitrile, ultrapure water, and acetic acid in a ratio of 79:20:1 (*v/v/v*), was added to each tube. The tubes were then transferred to a shaker plate and placed

on a rotary shaker at 600 rpm and 25 °C for 90 min (miniShaker VWR; VWR, Leighton Buzzard, UK). After shaking, the extracts were centrifuged for 5 min at 15,500×*g* (Centrifuge 5417S Eppendorf, Stevenage, UK) at 24 °C. The supernatants (75 μL) were mixed with 75 μL of dilution solvent, which contains acetonitrile, ultrapure water, and acetic acid in a ratio of 20:79:1 (*v/v/v*) and transferred to vials with 250 μL microinserts.

2.1.4. LC-MS/MS procedure

Analysis by LC-MS/MS was performed using an Exion series LC system coupled to a 6500+ hybrid triple quadrupole-linear ion trap mass spectrometer (qTRAP-MS) system and to an IonDrive Turbo Spray (both Sciex Technologies, Warrington, UK). Chromatographic separation was achieved on a reversed-phase ACE-3 C18 column (2.1 × 100 mm, 3 μm particle size; Hichrom, Berkshire, UK) equipped with an ACE-3 guard cartridge maintained at 60 °C. The gradient elution was carried out with solvent A, which contained ultrapure water, methanol and acetic acid in a ratio of 89:10:1 (*v/v/v*) and solvent B, which contained ultrapure water, methanol and acetic acid in a ratio of 2:97:1 (*v/v/v*), both supplemented with 5 mM ammonium acetate to promote the formation of ammonium adducts. The applied gradient was 20 min long as described: 0 min, 0 % B; 2 min, 0 % B; 5 min, 50 % B; 14 min, 100 % B; 18 min, 100 % B; 19 min 0 % B. Flow rate was set at 0.6 mL/min and the injection volume was 1 μL.

The MS analysis operated in positive (ESI+) and negative (ESI-) electrospray ionisation (ESI) modes depending on the mycotoxin studied. The source conditions were set as follows: curtain gas 40 psi, collision gas medium, ion spray voltage −4500 V (in negative) and 5500V (in positive), temperature 400 °C, ion source gas 1 60 psi and ion source gas 2 60 psi. The multiple reaction monitoring (MRM) acquisition mode was applied. The optimised retention time, precursor ion and product ions obtained via direct infusion (syringe method) of reference standard solutions for the studied mycotoxins are reported in Table 1. The MS/MS parameters (collision energy, declustering potential, entrance potential and collision cell exit potential), presented also in Table 1, were also optimised by infusion on each compound separately and checked on the mix stock standard solution. Two or three m/z transitions were monitored for each mycotoxin. The analyte identification was based on the assessment of retention time and the quantifier and qualifier transitions. Data were acquired using Analyst® software version 1.6.3 and quantified with MultiQuant™ version 3.0.3.

2.1.5. Method validation

The LC-MS/MS method for quantifying T-2+HT-2 in individual oat grains was validated by the Commission Regulation (EU) 2023/2782 (European Commission, 2023, pp. 1–44) and the guidance provided by Wenzl et al. (2016) for determining method performance characteristics in food contaminant analysis. Selectivity was assessed by injecting standard solutions of each mycotoxin (1 μL) in triplicate and monitoring the retention time and peak shape for consistency. To verify the absence of matrix interferences, blank matrix extracts, matrix-matched standards, and spiked samples were analysed. The presence of co-eluting signals at the monitored m/z transitions was also checked, ensuring specific and reliable analyte detection. Linearity was evaluated by preparing matrix-matched calibration curves consisting of nine concentration levels for each analyte, covering the expected range in oat grains. Each level was analysed in duplicate. The calibration curves were constructed by plotting peak area versus concentration, and linearity was verified by calculating the coefficient of determination (R^2), with a predefined acceptance criterion of $R^2 \geq 0.98$. Precision and recovery were evaluated through spiking experiments on blank ground oat grains. Three different validation batches were performed on separate days. For each batch, grains were spiked at 250 μg/kg (T-2) and 750 μg/kg (HT-2). A total of 16 replicates (n = 3, 3, 10) were processed using the defined extraction and analytical protocol. Precision was expressed as the relative standard deviation (RSD), and trueness was assessed by calculating the percentage recovery of each toxin (Table 1). Method sensitivity was evaluated by estimating the limits of detection (LOD) and quantification (LOQ) using the pseudo-blank approach described by Wenzl et al. (2016) (Table 1). To account for potential matrix effects, all calibration standards were prepared using blank matrix extracts, and blank matrix injections were included in the analytical batch. Matrix-matched calibration ensured consistent quantification and reduced signal variability due to ion suppression or enhancement.

2.2. Spectroscopy setup

2.2.1. NIR-HSI

A push-broom hyperspectral imaging system composed of a Pika NIR-320 camera assembled by Resonon Inc. (Bozeman, MA, USA) was used. The device consists of an InGaAs sensor line scan camera with a 320 × 256-pixel resolution, 14-bit resolution A/D spectrograph and 30 × 30 μm pixel size (Goldeye G-008 SWIR TEC1, Allied Vision Technologies GmbH, Germany). The spectral resolution was 4.6–4.7 nm (164 spectral channels per pixel from 900 nm to 1700 nm), with a spatial resolution of 320 pixels. The objective lens had a focal length of 25 mm (F/1.4 SWIR, 0.9–1.7 μm, 21 mm image format, c-mount), which was positioned 220 mm above the image surface. The illumination unit was composed of four halogen lamps with Lambertian filters fixed onto an adjustable tower that was turned on at least 20 min before image acquisition. The illumination system was powered by a Samplexpower® power converter (SEC-1223CE, Burnaby, BC, V5A 0C6, Canada), which provides a highly regulated output DC voltage of 13.8 V at 23 Amps with an AC input of 230 V, 50 Hz. Finally, a motorised linear translation stage with a range of 600 mm was also used, allowing the sample to move while the optical system remained stationary.

Spectronon PRO software was used to control Resonon's benchtop for image processing. The raw reflectance readings for each sample data array were corrected by dividing the dark current-subtracted reflectance by the dark current-subtracted white standard reflectance at each corresponding wavelength (1). A dark current intensity image was collected before sample scanning to remove dark current noise by covering the camera lens. In addition, the intensity from a 99 % white reflectance standard, made of polytetrafluoroethylene (Spectralon™, SRT-99-120, Labsphere, North Sutton, NH, USA), was collected immediately after the dark current image to correct illumination effects. These two images were applied to subsequent sample intensity images.

$$I = \frac{I_0 - I_b}{I_w - I_b} \quad (1)$$

Table 1
Optimised liquid chromatography-tandem mass spectrometry parameters (LC-MS/MS) for the quantification of T-2 and HT-2 toxins in unprocessed oat grains and their analytical performance. LOD = limit of detection; LOQ = limit of quantification; SD = standard deviation; RSD = relative standard deviation.

Mycotoxin	Retention time (min)	Precursor ion (*m/z*)	Molecular ion	Product ions (*m/z*)[1]	Collision energy (V)	Declustering potential (V)	Entrance potential (V)[2]	Collision cell exit potential (V)	LOD/ LOQ (μg/L)	Recovery ± SD, %	RSD, %
HT-2 toxin	6.06	442.0	$[M + NH_4]^+$	**262.9** 215.0	17	1	–	24 12	1.2/4.0	114.6 ± 6.5	5.6
T-2 toxin	6.58	484.0	$[M + NH_4]^+$	**305.0** 215.1	19 27	26	–	14 12	0.2/0.8	119.2 ± 3.7	3.2

where I_0 is the raw hyperspectral image obtained, I_w is the white reference, and I_b is the dark current reference. Besides the dark and absolute reflectance response, the pixel illumination saturation was also adjusted with the camera controls. The framerate and the integration time were established so that no pixel on the image was saturated.

For the oat individual grain analysis (200 grains, 100 from each sample set), each grain was scanned without any specific template, and the mean spectrum was recorded. This process was repeated in triplicate, changing the grain orientation in face-up, face-down and random position. Once the spectra (600 spectra) were recorded, the grains were used for T-2+HT-2 analysis.

In all the cases, a black tray was used to reduce the background noise in the image and to obtain an accurate pixel selection. Images were adjusted to 350 bands for the x-axis and approximately 90 mm for the y-axis. Pixel selection of the oat grains was done by collecting the mean reflectance values of similar spectrum pixels by Euclidean distance, which is best adjusted to the region of interest to remove the background signal. The mean spectrum for each grain was recorded as a text file for later exporting to the spectral analysis software.

2.2.2. Vis-NIR

The spectra for the same oat individual grains were collected with grains in face-up, face-down and random positions. Therefore, each of the 200 grains was scanned three times in different orientations, resulting in a total of 600 spectra. A LabSpec 2500® Near-Infrared Analyser (350–2500 nm; Analytical Spectral Devices Inc., USA) was used for spectral acquisition. The system included three detectors: one silicon array (350–1000 nm) and two Peltier-cooled InGaAs detectors (1000–1800 nm and 1800–2500 nm), with a sampling interval of 1 nm. Oat grains were positioned directly against a fibre-optic probe connected to an internal quartz-halogen light source (Ocean Optics, USA), and spectra were acquired in digital number mode. To reduce external light interference, a sample tray and a black bottle cap were used.

The system was powered on 50 min before measurements to ensure stability and accuracy. A Spectralon® Diffuse Reflectance Standard was used for calibration before starting the measurements, and after every ten grains. Additionally, a baseline was recorded, and three preliminary spectra were taken to verify measurement consistency.

The spectroscopy setup consisted of the LabSpec analyser, an interactance probe connected to the light source, and a computer running Indico Pro image acquisition software (Malvern Panalytical Ltd, Malvern, UK).

2.3. Data processing

The collected spectral data were processed to develop classification models for detecting contaminated grains. The process included spectral preprocessing, model training, and validation. All analyses were conducted using Python 3.11.10 with Scikit-Learn 1.6.1 for classification, Imbalanced-Learn 0.13.0 for oversampling, and additional libraries, including Numpy 2.0.1, Scipy 1.15.1, and Pandas 2.2.3.

2.3.1. Spectral preprocessing

First, the spectral differences between grains contaminated above and below the EU legal limit (1250 μg/kg) and above and below 10,000 μg/kg were observed. The mean spectral profiles for each category were generated with Python version 3.11.10.

The spectral data were initially organised into two distinct datasets before applying any preprocessing techniques. A total of 600 spectra (200 grains scanned three times) were acquired by NIR-HSI (900–1700 nm), while another 600 spectra (200 grains scanned three times) were collected for Vis-NIR (350–2500 nm). To minimise scattering effects, the extremes of each dataset were removed, resulting in a range of 1000–1600 nm for NIR-HSI and 380–2470 nm for Vis-NIR.

To assess the impact of different preprocessing techniques on classification performance, several preprocessing strategies were applied to the datasets. Initially, the raw spectral data were retained as a baseline for comparison. Standard normal variate (SNV) correction was applied to some datasets to mitigate multiplicative scattering effects and standardise spectral intensities. Additionally, the first derivative of the spectra was computed to enhance subtle spectral features and remove baseline offsets. Two sequential combinations of these techniques were also explored: computing the first derivative followed by SNV correction and applying SNV correction before computing the first derivative. These five strategies were evaluated to determine the most effective approach for improving the discriminative power of spectral features in detecting T-2+HT-2 contamination in oat grains.

2.3.2. Chemometric modelling

To address class imbalance between contaminated and non-contaminated grains, the synthetic minority over-sampling technique (SMOTE) was applied using Imbalanced-Learn 0.13.0. This technique generated synthetic samples for the minority class, ensuring an equal number of samples per class and enhancing the robustness and generalisability of the classification model.

For classification, toxin concentration measurements were converted into binary outcomes. Two thresholds were selected to reflect different practical objectives: 1250 μg/kg, corresponding to the EU legal limit, and 10,000 μg/kg, used as a target to efficiently reduce the overall toxin burden by removing only the most contaminated grains. For each threshold, samples above the limit were labelled as contaminated (1), and the rest as non-contaminated (0). This allowed the evaluation of classification performance under both regulatory and mitigation-focused criteria. Several classifiers were evaluated, including Logistic Regression, Decision Tree, Support Vector Machine, Random Forest, and K-Nearest Neighbours, all implemented using Scikit-Learn 1.6.1. A leave-one-out cross-validation approach was employed, where each spectrum was sequentially excluded from the training set in each iteration. This process was repeated for every spectrum, and the overall classification accuracy (CA) was computed. In total, for NIR-HSI, 2 thresholds x 5 models x 5 preprocessing techniques resulted in 50 models, and the same number of models was generated for Vis-NIR.

Moreover, the top 20 most important spectral features were identified and visualised using bar plots for the 20 best-performing models. Given the superior performance of the Random Forest model, these top 20 features were used to develop refined models using only the three best preprocessing techniques, optimising CA with a reduced feature set.

2.3.3. Model validation

The best-performing classifiers were identified based on CA for each preprocessing technique, spectroscopy method, and threshold. Confusion matrices were generated for these selected models (10 per spectroscopic method) to analyse correct and wrong classifications. Additionally, receiver operating characteristic and precision-recall curves were plotted, allowing computation of the area under the receiver operating characteristic curve (AUC) and evaluation of precision-recall trade-offs. The optimal models exhibited high CA with strong true positive and true negative predictive rates, with AUC values approaching 1.0, while models with AUC values near 0.5 were considered random classifiers. In all cases, the Random Forest model outperformed the other classifiers.

2.4. Sampling statistical analysis

The statistical analyses and graphical displays were performed using RStudio version 4.2.3 (Posit, MA, USA) and Microsoft Excel version 16.87 (Microsoft, Redmond, Washington). To calculate the overall average and median contamination for each T-2+HT-2, a value of LOD/$\sqrt{2}$ was used for grains with values below the LOD (Hites, 2019). Theoretical and empirical approaches were employed to assess the probability that the average levels of the sum of T-2+HT-2 in oat

samples selected from different percentages of grains exceeded the EU thresholds (1250 μg/kg). Firstly, to calculate the theoretical probability of accepting or rejecting the oat batch samples, the distribution of the dataset—consisting of toxin levels measured in individual oat grains—was analysed. Secondly, the log-normal distribution was the best fit according to QQ-Plots, Cumulative Distribution Function plots, and PP-Plots. Subsequently, randomly selected grains (from the 200 grains analysed), ranging from 0.5 % to 100 % of the total dataset, were drawn with replacement to calculate theoretical and empirical probabilities. For each percentage of selected grains, 100 iterations were conducted, following a subsampling approach inspired by the EU regulations for cereal batches (European Commission, 2023, pp. 1–44), but applied here to individual grains within a sample. In each iteration, the mean toxin level was calculated. The probability of exceeding the thresholds was determined by the proportion of iterations where the mean surpassed the specified limit. The empirical method provided a distribution-free estimation and used the original dataset, contrasting with the theoretical approach based on the log-normal assumption of the data.

3. Results and discussion

3.1. Performance of the analytical method

The LC-MS/MS method used for T-2+HT-2 analysis was successfully validated. Recovery rates were within satisfactory limits, and the RSDs met the acceptable criteria of 70–120 % established by Commission Regulation (EC) No. 2023/2782 (European Commission, 2023, pp. 1–44), as shown in Table 1. Calibration curves for both mycotoxins exhibited excellent linearity, with R^2 exceeding 0.99. The method also demonstrated high sensitivity, with low LOD and LOQ, enabling the reliable identification of trace levels. Additionally, matrix effects were negligible due to the use of matrix-matched calibration and the injection of blank matrix samples.

3.2. T-2 and HT-2 toxins concentration distribution in oat grains

Fig. 1 illustrates the frequency distribution of T-2+HT-2 concentration in individual oat grains from sample set 1, sample set 2, and the combined dataset, as determined by LC-MS/MS. An expanded view highlights grains with toxin levels exceeding 2000 μg/kg. The results reveal a highly skewed distribution, with most grains exhibiting low toxin concentrations, while a smaller proportion contains significantly higher levels. It is important to note that the two sample sets analysed in this study were pre-selected based on their known high T-2+HT-2 content (as detailed in Section 2.1.1). Therefore, the observed toxin distribution reflects these specific samples and should not be interpreted as representative of the general oat population.

A total of 43 grains (21.5 %) exceeded the legal limit of 1250 μg/kg, highlighting the presence of a substantial number of highly contaminated grains. Furthermore, 22 grains (11 %) had toxin concentrations greater than 10,000 μg/kg, indicating extreme contamination in a subset of grains. The highest concentration detected was 335,256 μg/kg, suggesting the presence of exceptionally contaminated grains within the sample. The average toxin concentration across the 200 individually analysed grains was 10,123 μg/kg, which is notably higher than the concentrations reported for the bulk composite samples from which they were drawn (3400 μg/kg and 3120 μg/kg for sample sets 1 and 2, respectively). This discrepancy underscores the impact that a small number of highly contaminated grains can have on the overall toxin load. In contrast, the median toxin concentration was 214 μg/kg, and the minimum concentration detected was below the LOD, reinforcing the skewed nature of the distribution.

A similar trend has been observed in a previous study investigating

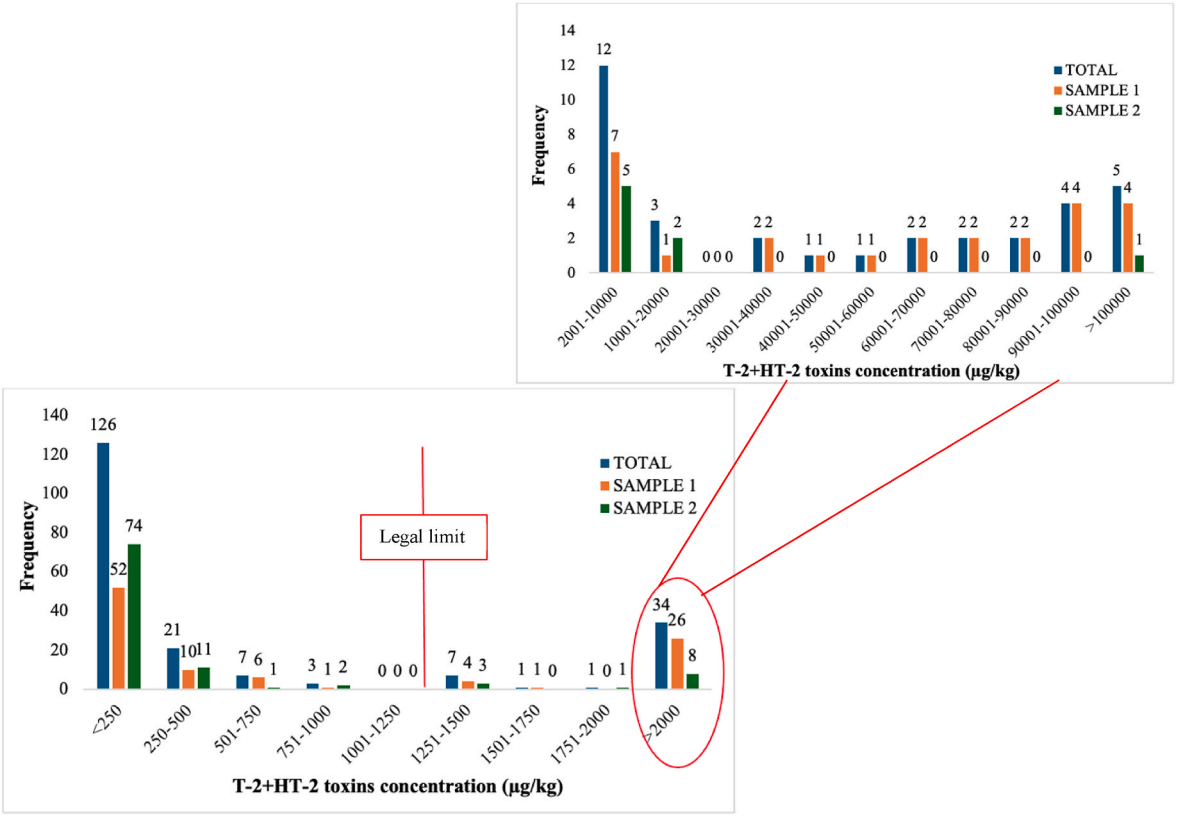

Fig. 1. Distribution of T-2+HT-2 toxins content (μg/kg) in oat unprocessed grains from sample set 1, sample set 2, and the combined dataset. An expanded view highlights grains with toxins level exceeding 2000 μg/kg. The red line indicates the legal limit for T-2+HT-2 toxins content.

oat samples with high DON content, where only 8 % of the individual grains exceeded the contamination EU threshold (1750 μg/kg) (Teixido-Orries, Molino, Castro-Criado et al., 2025). Likewise, Femenias et al. (2022) reported a similar pattern in wheat grains from samples with high DON content, further reinforcing the heterogeneous distribution of mycotoxins in cereal grains.

3.3. Comparison of spectral profiles of oat grains with different T-2 and HT-2 toxin levels

Fig. 2 presents the mean spectral profiles of oat grains with different levels of T-2+HT-2, analysed using NIR-HSI and Vis-NIR spectroscopy. Fig. 2A and C compare the spectral responses of oat grains with toxin concentrations above and below the legal threshold of 1250 μg/kg; meanwhile, Fig. 2B and D illustrate the spectral variations between grains exceeding or remaining below 10,000 μg/kg.

A clear distinction is observed in the degree of spectral overlapping between the two contamination thresholds. In the case of the 1250 μg/kg limit (Fig. 2A and C), the spectra of contaminated and uncontaminated grains exhibit significant overlap, indicating relatively subtle spectral differences. This suggests that at lower contamination levels, the changes in oat grains caused by mycotoxin production have a less noticeable impact on their spectral properties, making it harder to distinguish them. Conversely, at the higher contamination threshold of 10,000 μg/kg (Fig. 2B and D), the spectral profiles of the two groups diverge more noticeably, with greater differences in reflectance and digital number intensities across specific wavelength regions. This potentially indicates that as the toxin concentration increases, the alterations in the chemical and physical composition of the oat grains become more evident, leading to a stronger spectral response.

The most pronounced spectral differences between contaminated and uncontaminated oat grains are observed in specific wavelength regions. In the Vis (400–700 nm), the digital numbers of grains with lower toxin levels are generally lower; meanwhile, in the NIR-HSI spectra (1000–1600 nm), oat grains with higher toxin concentrations tend to exhibit lower reflectance values. These findings align with previous research on spectral variability associated with mycotoxin contamination in cereals. In a previous study, some overlap was observed in the NIR region between oat samples contaminated with T-2+HT-2 at levels above and below 1000 μg/kg, like the overlapping trends observed in a study at the 1250 μg/kg threshold (Teixido-Orries, Molino, Gatius, et al., 2023). However, at higher contamination levels (10,000 μg/kg), the spectral differences became more pronounced. This is consistent with findings by Alisaac et al. (2019), who observed increased spectral reflectance across the Vis-NIR range in wheat kernels infected with *F. graminearum*. Although *F. graminearum* and *F. langsethiae* differ notably in their pathogenicity mechanisms and the type of mycotoxins they produce (type B trichothecenes vs. type A, respectively), these results support the general premise that fungal infection, regardless of species, can induce detectable spectral changes in cereal grains. Similarly, Delwiche et al. (2011) found significant Vis-NIR spectral differences between damaged and undamaged wheat grains infected by *Fusarium*. A different trend was reported by Tekle et al. (2013), who found that the spectral profiles of low- and high-DON oat samples were quite similar. However, low-DON samples exhibited lower absorption in the Vis and higher absorption in the NIR regions compared to high-DON samples, a pattern also observed in our results for T-2+HT-2 contamination.

However, due to the complexity of the spectral data and the overlapping signals, data pre-processing and chemometric tools were

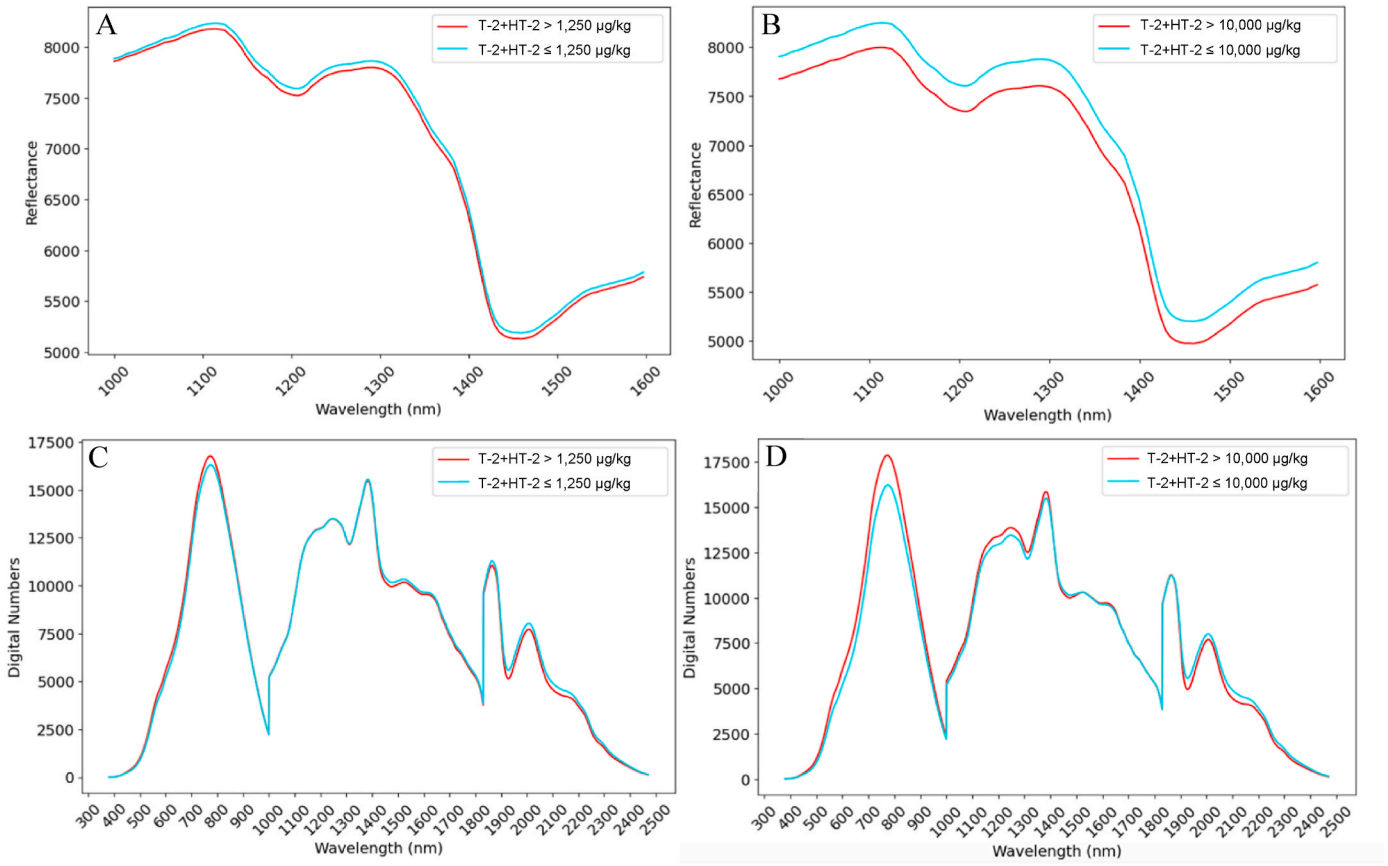

Fig. 2. Mean spectral profiles of oat kernels with T-2+HT-2 toxins level above and below the legal limit of 1250 μg/kg, obtained using NIR-HSI (A) and Vis-NIR spectroscopy (C). Spectral profiles of oat kernels with T-2 and HT-2 toxins (T-2+HT-2) levels above and below 10,000 μg/kg are also shown using NIR-HSI (B) and Vis-NIR spectroscopy (D).

required to extract valuable spectral information and improve discrimination between grains.

3.4. Classification of individual oat grains according to the EU legal limit (1250 μg/kg)

Table 2 presents the results of the 10 highest-performing classification models (all obtained using the Random Forest algorithm) for discriminating individual unprocessed oat grains according to the EU legal limit (1250 μg/kg) for T-2+HT-2, using NIR-HSI and Vis-NIR spectroscopy with various pre-processing techniques. The CA varied depending on the pre-processing applied, with higher performance observed in models using spectral normalisation techniques and first derivative transformation. For NIR-HSI, raw data resulted in the lowest CA (82.7 %), whereas applying pre-treatments significantly improved model performance. The best model was obtained using the first derivative combined with SNV, achieving a CA of 93.0 % and an AUC of 0.98. Other effective pre-treatments included SNV alone (CA = 89.5 %) and the first derivative alone (CA = 90.1 %). In the case of Vis-NIR, raw data CA was slightly higher (83.8 %) than that of raw NIR-HSI. However, pre-treatments again improved classification performance, with the best model (SNV + first derivative) achieving 89.4 % CA and an AUC of 0.97. Overall, NIR-HSI outperformed Vis-NIR, particularly after pre-processing, which highlights its ability to capture detailed chemical and structural information, whereas Vis-NIR is more sensitive to surface-related physical changes.

To our knowledge, the classification of individual cereal grains according to their content of T-2+HT-2 by spectroscopy has never been performed to date. Therefore, this is the first study that classifies naturally contaminated individual oat grains according to T-2+HT-2 content using spectroscopic techniques. In previous research, samples of naturally contaminated oat were classified based on their DON and T-2+HT-2 content, achieving maximum CAs of 83.2 % and 94.1 %, respectively (Teixido-Orries, Molino, Femenias, et al., 2023; Teixido-Orries, Molino, Gatius, et al., 2023), which were comparable to the results obtained in the present study. The only classification models for individual oat grains were developed by Tekle et al. (2015), who utilised NIR-HSI to classify individual pixels of artificially contaminated oat grains based on *Fusarium* damage and DON content. Their approach involved calculating the ratio of damaged pixels per grain to differentiate between symptomatic categories and DON levels. Their findings demonstrated that NIR-HSI could detect grains with high DON content, even if they

Table 2
Classification accuracies (CAs), confusion matrix, area under the curve (AUC) and most characteristic wavelengths for validation sets in the classification models of unprocessed oat grains according to the European Union (EU) legal limit (1250 μg/kg) of T-2 and HT-2 toxins. U = grains above the legal limit; L = grains below the legal limit.

Equipment	Pre-treatment	Confusion matrix (%)			CA (%)	AUC	Most characteristic wavelength (nm)
NIR-HSI (1000–1600 nm)	Raw data	Actual	Predicted		82.7	0.90	1399
			U	L			
		U	87	13			
		L	22	78			
	SNV	Actual	Predicted		89.5	0.96	1523
			U	L			
		U	92	8			
		L	13	87			
	1st derivative	Actual	Predicted		90.1	0.97	1450
			U	L			
		U	93	7			
		L	12	88			
	1st derivative + SNV	Actual	Predicted		93.0	0.98	1481
			U	L			
		U	96	4			
		L	10	90			
	SNV + 1st derivative	Actual	Predicted		91.8	0.98	1445
			U	L			
		U	94	6			
		L	10	90			
Vis-NIR (380–2470 nm)	Raw data	Actual	Predicted		83.8	0.93	460
			U	L			
		U	90	10			
		L	25	75			
	SNV	Actual	Predicted		82.6	0.92	531
			U	L			
		U	88	12			
		L	23	77			
	1st derivative	Actual	Predicted		88.9	0.97	432
			U	L			
		U	93	7			
		L	15	85			
	1st derivative + SNV	Actual	Predicted		89.8	0.97	1660
			U	L			
		U	94	6			
		L	14	86			
	SNV + 1st derivative	Actual	Predicted		89.4	0.97	438
			U	L			
		U	94	6			
		L	15	85			

appeared asymptomatic. Nevertheless, these authors used artificially contaminated oats and did not classify individual oat grains according to the EU legal limit of DON. Furthermore, since their study involved *F. graminearum*, it is important to highlight that this species differs substantially from *F. langsethiae* in its pathogenicity and mode of infection in oats. These biological differences may impact how the infection manifests in the grain and therefore affect the performance or relevance of the classification models used. Other studies have classified individual cereal kernels for DON screening in accordance with the EU legal limit, reporting CAs of 79.2 % for wheat (Barbedo et al., 2017) and 79.5 % for barley (Su et al., 2021). While classification of individual grains according to DON content has been extensively investigated, specific studies focusing on T-2+HT-2 remain scarce. The present work contributes to filling this gap by targeting these toxins specifically in oats, but further research is still needed to consolidate current findings and develop robust models applicable across different contamination scenarios.

T-2+HT-2 concentration found in oats is low compared with the principal constituents of the grain (starch, protein, water, etc.). Consequently, these mycotoxins cannot be detected directly by Vis-NIR and NIR-HSI. Classification based on mycotoxins relies on structural and chemical changes induced by *Fusarium* growth and toxin synthesis. The Vis region is particularly useful for detecting physical characteristics such as defects, discolouration, and structural damage, while the NIR regions are more commonly used for analysing chemical composition, structural feature changes and moisture content (Walsh et al., 2020). This fact explains why the Vis and NIR regions can be used for trichothecene detection in cereals, though with different mechanisms.

The NIR region plays a crucial role in spectral analysis, particularly when employing NIR-HSI. In this study, the most characteristic wavelengths in the NIR region for T-2+HT-2 detection were found in the 1400–1520 nm range. Other authors, such as Yan et al. (2017), investigated oat traits correlated with high DON content, another trichothecene mycotoxin produced by *Fusarium* species. Their findings indicated that oat cultivars highly contaminated with DON exhibited higher protein content and a greater hull-to-groat ratio. However, the relationship between chemical and physical changes in oat grains and elevated T-2+HT-2 contamination remains unclear. Martin et al. (2018) reported that *F. langsethiae*, which is the primary global producer of T-2+HT-2, induces alterations in β-glucans content. These findings suggest that the ability of NIR-HSI to discriminate T-2+HT-2 contaminated grains could be linked to changes in these fundamental oat components. In previous research, the most relevant wavelengths for predicting T-2+HT-2 contamination in oat samples were identified: 1038, 1052, 1110, 1144, 1393, and 1481 nm (Teixido-Orries, Molino, Gatius, et al., 2023). These wavelengths fall within the NIR range observed in the present study, reinforcing the potential of NIR spectroscopy for mycotoxin detection. The complexity of NIR spectra in oat grains arises from multiple overtone vibrations and band combinations associated with organic bonds, including C-H (aliphatic and aromatic), O-H, C-O, and N-H (amide and amine) (Meenu et al., 2022). Specifically, spectral bands around 1400 nm correspond to the combination of C-H and O-H first overtones, while the 1480 nm band is associated with the N-H first overtone (Badr Eldin, 2010). C-H bonds are primarily linked to carbohydrates, O-H bonds are present in most organic molecules and water, and N-H bonds are mainly associated with proteins. Meenu et al. (2022) successfully quantified β-glucan in hulled oats using NIR spectroscopy (700–2500 nm), identifying a strong correlation between β-glucan content and wavelengths in the 1225–1440 nm range. Additionally, previous studies have related the 1400 nm band to *Fusarium*-induced damage in cereals (Delwiche et al., 2019; Tekle et al., 2013). Given that *F. langsethiae* infection alters β-glucans level, protein content and hull-to-groat ratio in oat grains through fungal growth and mycotoxin synthesis, it is plausible that these modifications contribute to the predictability of T-2+HT-2 using the NIR region.

The analysis also highlighted that certain wavelength regions within the Vis spectra showed high CA values according to T-2+HT-2 concentration when using Vis-NIR spectroscopy. The region that included the most characteristic wavelengths was 430–530 nm. Interestingly, previous studies have reported similar findings. Tekle et al. (2013) found that the spectral wavelengths that were one of the most effective for distinguishing between low-DON and high-DON oat ground samples were around 492 nm. Similarly, Delwiche et al. (2011) identified significant spectral differences between *Fusarium*-damaged and undamaged wheat kernels at 502 nm using HSI Vis-NIR. These findings align with our results, particularly in the Vis region, reinforcing the relevance of these wavelengths for detecting mycotoxin contamination. Although the oats analysed in this study were naturally contaminated, previous research suggests that artificial contamination increases the likelihood of darkening. For instance, Tekle et al. (2013) reported a slight darkening in oat samples artificially contaminated with DON. This darkening, although not always visually perceptible, is likely associated with the brownish discolouration commonly observed in the hulls and caryopses of *Fusarium*-infected oats. Such discolouration may enhance spectral differentiation in the Vis (Fig. 2) region, thereby improving the accuracy of models for T-2+HT-2 classification.

Therefore, the classification of oat grains based on their T-2+HT-2 content by spectroscopy can be as viable as the classification of different cereals according to their content in other trichothecenes.

3.5. Classification of individual oat grains according to a T-2 and HT-2 toxins level of 10,000 μg/kg

Table 3 shows the classification performance of individual oat grains at a higher contamination threshold (10,000 μg/kg) (all of them also obtained with the Random Forest algorithm). Compared to the models developed for the EU legal limit (1250 μg/kg), the CAs for this threshold were generally higher across all pre-processing techniques, indicating that increased contamination results in more distinct spectral differences as observed in Section 3.3. For NIR-HSI, raw data CA improved to 85.7 %, and the best model (SNV + first derivative) achieved a 97.1 % CA with an AUC of 1.00. Similarly, the first derivative + SNV model performed exceptionally well (96.2 % CA, AUC = 1.00), reinforcing the significance of pre-processing techniques in enhancing spectral feature extraction. Vis-NIR models also exhibited enhanced performance at this higher contamination level, with the best model (SNV + first derivative) reaching 98.0 % CA. The performance improvements at 10,000 μg/kg suggest that contamination-induced changes become more prominent at higher toxin levels, making grains easier to classify.

The improved performance of these models aligns with the spectral trends observed in Fig. 2, where more distinct differences were seen between grains classified according to the 10,000 μg/kg threshold. The higher accuracy in this Section 3.5 may be due to the greater variability in spectral patterns at higher toxin levels, allowing models to capture subtle differences more effectively. Additionally, at 1250 μg/kg, the spectral characteristics of contaminated grains may be more homogeneous, potentially reducing the model's ability to distinguish variations within this category. At this higher contamination threshold, Vis-NIR slightly outperformed NIR-HSI, likely due to the contribution of the Vis region in capturing possible grain darkening associated with severe fungal infection. This suggests that, when contamination levels are extreme, physical changes in the grain can become more pronounced and detected using Vis-NIR spectroscopy.

Similar wavelengths to those identified in Section 3.4 were also relevant in the 1400–1520 nm range for obtaining the present results. Likewise, in the Vis region, wavelengths within the 430–580 nm range were significant, leading to comparable conclusions. Additionally, the 1203 nm wavelength emerged as an important feature in these models. The spectral band at 1144 nm corresponds to the second overtone of C-H bonds (Badr Eldin, 2010), which is primarily associated with carbohydrates. Serranti et al. (2013) explored the use of NIR-HSI to classify oat and groat (hull-less oat) and identified three key wavelengths in their

Table 3
Classification accuracies (CAs), confusion matrix, area under the curve (AUC) and most characteristic wavelengths for validation sets in the classification models of oat grains according to the 10,000 μg/kg threshold of T-2 and HT-2 toxins. U = grains above the threshold; L = grains below the threshold.

Equipment	Pre-treatment	Confusion matrix (%)			CA (%)	AUC	Most characteristic wavelength (nm)
NIR-HSI (1000–1600 nm)	Raw data	Actual	Predicted		85.7	0.93	1409
			U	L			
		U	90	10			
		L	18	82			
	SNV	Actual	Predicted		93.4	0.99	1512
			U	L			
		U	98	2			
		L	10	90			
	1st derivative	Actual	Predicted		94.7	0.99	1450
			U	L			
		U	98	2			
		L	9	91			
	1st derivative + SNV	Actual	Predicted		96.2	1.00	1481
			U	L			
		U	99	1			
		L	6	94			
	SNV + 1st derivative	Actual	Predicted		97.1	1.00	1203
			U	L			
		U	99	1			
		L	1	95			
Vis-NIR (380–2470 nm)	Raw data	Actual	Predicted		89.8	0.97	455
			U	L			
		U	95	5			
		L	15	85			
	SNV	Actual	Predicted		91.8	0.97	580
			U	L			
		U	95	5			
		L	11	89			
	1st derivative	Actual	Predicted		96.2	1.00	439
			U	L			
		U	98	2			
		L	6	94			
	1st derivative + SNV	Actual	Predicted		97.1	1.00	439
			U	L			
		U	93	7			
		L	5	95			
	SNV + 1st derivative	Actual	Predicted		98.0	1.00	439
			U	L			
		U	98	2			
		L	2	98			

predictive models, two of which were around 1200 nm. This region, which also proved to be relevant for predicting T-2+HT-2 content in this study, is closely linked to C-H bonds. Furthermore, previous research has attributed wavelengths around 1200 nm to *Fusarium*-induced damage in cereals (Delwiche et al., 2019; Tekle et al., 2013). These findings further support the hypothesis that the alteration of hull-to-groat ratio and carbohydrate content, driven by fungal growth and mycotoxin synthesis, plays a critical role in detecting T-2+HT-2 using the NIR region.

These results reinforce the potential of spectroscopic techniques for precise regulatory compliance monitoring. By integrating NIR-HSI and Vis-NIR spectroscopy into industrial sorting systems, highly contaminated oat grains could be selectively removed, reducing waste and ensuring compliance with regulatory limits. The ability to classify individual grains instead of entire batches would represent a significant advancement for the cereal industry, optimising economic and food safety outcomes. However, scaling this approach to an industrial level would require further technological developments to enable real-time online separation, which remains an ongoing challenge.

3.6. Wavelength selection and multispectral classification models

The selection of the most relevant wavelengths plays a crucial role in optimising multispectral classification models for detecting T-2+HT-2 in oat grains. Table 4 highlights the 20 most frequently selected wavelengths across models, with the most recurrent ones being 432, 439, 440, 444, 445, 446, 455 in the Vis range, and 1000, 1193, 1203, 1208, 1213, 1419, 1424, 1445, 1450, and 1476 nm in the NIR range. Notably, these wavelengths align with those identified in Sections 3.4-3.5 and in the above-mentioned bibliography, reinforcing their importance in mycotoxin classification. A previously unmentioned wavelength of interest is around 1000 nm, which was also identified in previous research on oat samples (Teixido-Orries, Molino, Gatius, et al., 2023). Spectral bands between 1000 and 1100 nm correspond to the N-H and aromatic C-H first overtone, suggesting a probable association with carbohydrates and proteins.

To assess the effectiveness of these selected wavelengths, the top three pre-processing methods for each instrument and threshold were applied, and classification models were recalculated using only these 20 wavelengths. The CA obtained, presented in Table 5, shows a slight decrease compared to those in Tables 2 and 3. However, despite the significant reduction in model complexity, the maximum accuracy loss was limited to just 5.7 %. Reducing the complexity of the models to a multispectral dimension significantly simplifies their implementation, making them more practical for industrial applications (Wan et al.,

Table 4
Twenty most relevant wavelengths of the obtained classification models.

Equipment	Limit (μg/kg)	Pre-treatment	20 most relevant wavelengths
NIR-HSI (1000–1600 nm)	1250	Raw data	1399, 1414, 1010, 1000, 1005, 1419, 1038, 1409, 1429, 1440, 1424, 1019, 1393, 1029, 1476, 1450, 1388, 1404, 1014, 1497
		SNV	1523, 1419, 1518, 1424, 1512, 1528, 1533, 1409, 1549, 1000, 1507, 1019, 1560, 1414, 1476, 1010, 1144, 1024, 1247, 1497
		1st derivative	1450, 1076, 1445, 1081, 1455, 1193, 1033, 1072, 1168, 1173, 1134, 1208, 1213, 1471, 1038, 1149, 1005, 1465, 1043, 1460
		1st derivative + SNV	1481, 1486, 1476, 1491, 1471, 1465, 1353, 1327, 1332, 1586, 1512, 1591, 1450, 1134, 1129, 1445, 1358, 1125, 1597, 1173
		SNV+1st derivative	1445, 1076, 1465, 1476, 1072, 1129, 1125, 1450, 1471, 1081, 1173, 1067, 1591, 1363, 1120, 1460, 1455, 1287, 1327, 1358
	10,000	Raw data	1409, 1419, 1414, 1404, 1353, 1597, 1424, 1358, 1363, 1399, 1429, 1434, 1378, 1368, 1591, 1343, 1373, 1581, 1440, 1348
		SNV	1512, 1518, 1497, 1523, 1491, 1399, 1471, 1533, 1404, 1538, 1502, 1528, 1507, 1544, 1393, 1232, 1383, 1455, 1227, 1481
		1st derivative	1450, 1445, 1198, 1440, 1455, 1173, 1203, 1193, 1460, 1115, 1292, 1302, 1465, 1591, 1597, 1237, 1168, 1297, 1429, 1038
		1st derivative + SNV	1481, 1486, 1476, 1586, 1491, 1471, 1455, 1450, 1465, 1358, 1460, 1440, 1144, 1353, 1409, 1414, 1149, 1497, 1502, 1332
		SNV+1st derivative	1203, 1440, 1445, 1149, 1471, 1198, 1481, 1429, 1424, 1419, 1434, 1363, 1476, 1455, 1450, 1125, 1358, 1414, 1465, 1129
Vis-NIR (380–2470 nm)	1250	Raw data	460, 469, 448, 463, 476, 455, 431, 440, 458, 438, 457, 470, 426, 473, 441, 450, 462, 433, 432, 471
		SNV	531, 543, 2274, 1818, 2334, 501, 1993, 2285, 535, 2273, 2271, 536, 547, 2249, 2270, 546, 555, 2292, 548, 580
		1st derivative	432, 433, 437, 445, 439, 442, 438, 446, 444, 447, 449, 454, 455, 481, 482, 440, 436, 441, 470, 468
		1st derivative + SNV	1660, 444, 437, 1658, 1204, 1661, 1663, 430, 446, 1657, 440, 434, 455, 435, 441, 1670, 429, 432, 452, 439
		SNV+1st derivative	438, 455, 433, 449, 445, 444, 453, 439, 454, 443, 397, 505, 432, 501, 1254, 456, 1208, 532, 1210, 1209
	10,000	Raw data	455, 464, 446, 445, 466, 456, 470, 477, 432, 469, 458, 459, 460, 462, 468, 449, 465, 442, 470, 436
		SNV	580, 596, 537, 591, 582, 584, 545, 583, 577, 590, 596, 574, 536, 578, 575, 579, 586, 560, 599, 588
		1st derivative	439, 432, 445, 422, 444, 442, 440, 454, 437, 446, 450, 438, 433, 455, 481, 469, 436, 431, 470, 452
		1st derivative + SNV	439, 451, 445, 1656, 446, 432, 444, 422, 454, 438, 450, 431, 440, 447, 455, 452, 460, 464, 469
		SNV+1st derivative	439, 455, 445, 440, 444, 452, 1209, 1208, 776, 783, 464, 472, 1450, 456, 446, 2263, 540, 438, 506, 527

2020). If fewer wavelengths are used in the classification models, the rapid online application of T-2+HT-2 detection in highly contaminated oat grains becomes increasingly feasible.

A comparison between NIR-HSI and Vis-NIR spectroscopy highlights key differences in CA and model robustness. In general, NIR-HSI yielded higher CAs than Vis-NIR, particularly at the higher contamination threshold (10,000 μg/kg). The best-performing model for NIR-HSI at the 1250 μg/kg threshold was the 1st derivative pre-treatment, achieving a CA of 92.2 % with an AUC of 0.98. At the 10,000 μg/kg threshold, the 1st derivative model also showed the highest CA at 94.8 % (AUC = 0.99). For Vis-NIR, the CAs were slightly lower than those obtained with NIR-HSI, especially at the lower threshold. At the 1250 μg/kg threshold, the best-performing model was 1st derivative + SNV, which achieved a CA of 89.1 % with an AUC of 0.96. At the 10,000 μg/kg threshold, the highest CA was observed with 1st derivative + SNV, reaching 94.5 % with an AUC of 0.99. Although the accuracy of Vis-NIR models was lower than that of NIR-HSI, it remains a reliable alternative for mycotoxin classification.

3.7. Potential impact of observed results in sampling outcomes, regulatory compliance, and mycotoxin detection

Table 6 presents the empirical and theoretical probabilities of obtaining a T-2+HT-2 concentration in oat grains that exceeds the EU maximum limit of 1250 μg/kg, evaluated across different selected grain percentages. These probabilities were estimated using both empirical data and a log-normal model, considering a maximum of 200 grains (combined dataset). These results provide valuable insight into the potential implications of different sampling strategies for mycotoxin detection and food safety compliance.

The two analysed oat samples (calculated with the content in 100 grains each) showed an average toxin concentration above the EU legal threshold for T-2+HT-2. This result was consistent with the toxin levels measured in the corresponding subsamples of each sample, supporting the conclusion that the batches that contain these samples should be rejected by the food industry. However, statistical simulations demonstrated that the probability of detecting grains exceeding the legal limit increases as the percentage of selected grains rises. For instance, when only 0.5 % of the grains (equivalent to a single grain) were selected, the empirical probability of detecting contamination above the legal threshold was just 25 %. On the other hand, theoretical probability was slightly higher (33 %). As the proportion of selected grains increased to 5 %, the probability of surpassing the legal threshold rose to approximately 79–80 %, and full detection (100 %) was achieved when 30 % or more of the grains were sampled.

This pattern highlights the risk associated with small sample sizes, which may fail to detect highly contaminated grains, potentially leading

Table 5
Classification accuracies (CAs), confusion matrix and area under the curve (AUC) for validation sets in the classification of oat grains with redefined models using the 20 most relevant wavelengths according to the European Union (EU) legal limit (1250 μg/kg) and 10,000 μg/kg threshold of T-2 and HT-2 toxins. U = grains above the threshold; L = grains below the threshold.

Equipment	Limit (μg/kg)	Pre-treatment	Confusion matrix (%)				CA (%)	AUC
NIR-HSI (1000–1600 nm)	1250	1st derivative	Actual	Predicted			92.2	0.98
					U	L		
				U	96	4		
				L	12	88		
		1st derivative + SNV	Actual	Predicted			91.4	0.97
					U	L		
				U	94	6		
				L	12	88		
		SNV + 1st derivative	Actual	Predicted			90.7	0.97
					U	L		
				U	93	7		
				L	12	88		
	10,000	1st derivative	Actual	Predicted			94.8	0.99
					U	L		
				U	98	2		
				L	8	92		
		1st derivative + SNV	Actual	Predicted			93.5	0.99
					U	L		
				U	96	4		
				L	9	91		
		SNV + 1st derivative	Actual	Predicted			93.3	0.99
					U	L		
				U	97	3		
				L	11	89		
Vis-NIR (380–2470 nm)	1250	1st derivative	Actual	Predicted			86.7	0.94
					U	L		
				U	91	9		
				L	18	82		
		1st derivative + SNV	Actual	Predicted			89.1	0.96
					U	L		
				U	95	5		
				L	17	83		
		SNV + 1st derivative	Actual	Predicted			86.2	0.94
					U	L		
				U	91	9		
				L	19	81		
	10,000	1st derivative	Actual	Predicted			93.2	0.98
					U	L		
				U	97	3		
				L	11	89		
		1st derivative + SNV	Actual	Predicted			94.5	0.99
					U	L		
				U	99	1		
				L	10	90		
		SNV + 1st derivative	Actual	Predicted			92.3	0.98
					U	L		
				U	95	5		
				L	11	89		

to the acceptance of non-compliant batches. Given that mycotoxins are highly heterogeneous in individual oat grains, a small sample fraction may not adequately represent the contamination of the entire batch. This has significant implications for regulatory compliance, as conventional sampling approaches might underestimate contamination, allowing non-compliant products to enter the food supply chain.

From a risk mitigation perspective, it is noteworthy that if 21.5 % of the most contaminated grains were removed, the final toxin concentration would decrease to 218 μg/kg, well within legal limits. Similarly, eliminating the 11 % of grains with the highest contamination (>10,000 μg/kg) would reduce the final sample concentration to 624 μg/kg, also falling below the regulatory threshold. These findings underscore the importance of developing targeted strategies, such as spectroscopic techniques, to detect and remove highly contaminated grains. These strategies could significantly improve food safety and compliance with legal toxin thresholds.

This heterogeneity in mycotoxin distribution has been previously reported in oat grains from highly DON-contaminated samples, also with similar sampling conclusions obtained (Teixido-Orries et al., 2025). In this previous study, only a small percentage of grains contributed to most of the contamination, further supporting the need for improved sampling strategies that account for the uneven distribution of *Fusarium* mycotoxins in individual oat grains. Besides, although working with whole samples, Tittlemier and Whitaker (2023) suggested that current sampling plans for wheat and maize can introduce high variance in mycotoxin testing and risk of misclassifying consignments.

Overall, these results highlight the importance of optimising mycotoxin detection methodologies to ensure batch compliance with legal

Table 6
Empirical and estimated probabilities (0–1) of having a result over the European Union (EU) threshold for T-2+HT-2 toxins (1250 μg/kg) across the sampling of different percentages of oat grains (maximum number of grains = 200).

Percentage of sampled grains	Empirical probability		Predicted probability (lognormal model)	
	<1250 μg/kg	>1250 μg/kg	<1250 μg/kg	>1250 μg/kg
0.5 %	0.75	0.25	0.67	0.33
1 %	0.67	0.33	0.54	0.46
2 %	0.49	0.51	0.40	0.60
3 %	0.36	0.64	0.33	0.67
4 %	0.29	0.71	0.26	0.74
5 %	0.21	0.79	0.20	0.80
6 %	0.21	0.79	0.20	0.80
7 %	0.17	0.83	0.13	0.87
8 %	0.15	0.85	0.11	0.89
9 %	0.11	0.89	0.07	0.93
10 %	0.08	0.92	0.04	0.96
15 %	0.05	0.95	0.02	0.98
20 %	0.01	0.99	0	1
25 %	0.01	0.99	0	1
30 %	0	1	0	1
40 %	0	1	0	1
50 %	0	1	0	1
75 %	0	1	0	1
100 %	0	1	0	1

limits. Reducing the proportion of grains analysed may underestimate contamination levels, increasing the risk of accepting non-compliant batches. In this case, the studied oat batch would have to be rejected by the industry due to exceeding the legal threshold, reinforcing the need for enhanced detection and new sorting approaches (as spectroscopic techniques). These improvements would contribute to better compliance with EU regulations, minimising consumer exposure to harmful mycotoxins and reducing unnecessary food waste.

4. Conclusions

This study confirms that both Vis-NIR spectroscopy and NIR-HSI are effective, non-destructive methods for detecting T-2+HT-2 contamination in individual oat grains. The classification models developed achieved high accuracy, often exceeding 90 %, highlighting their potential for precise and targeted screening. Reducing the number of wavelengths to just 20 resulted in only a 5.7 % drop in CA. This simplification improves computational efficiency, supporting the feasibility of real-time applications in industrial settings. Moreover, the analysis of the spectral regions revealed that the Vis range mainly captures physical changes such as grain discolouration, while the NIR range detects chemical and structural alterations linked to *Fusarium* infection and toxin production.

Only 11 % of the grains exceeded 10,000 μg/kg, and their targeted removal using these techniques could reduce the total toxin concentration by 90 %, bringing levels below the EU legal limit and ensuring batch compliance. The findings also illustrate the limitations of traditional batch sampling. Simulated scenarios showed that analysing just 0.5 % of a batch may result in only a 25–33 % chance of detecting contamination above the regulatory limit. In contrast, sampling 30 % of grains consistently ensured detection, reinforcing the need for improved, grain-specific detection approaches.

Altogether, this work demonstrates the potential of Vis-NIR and NIR-HSI technologies to transform mycotoxin control in the oat industry. Their adoption could reduce economic losses, increase food safety, and support more sustainable production practices. Future research should aim to expand contamination datasets, validate models across different oat varieties, and optimise integration into industrial sorting systems.

CRediT authorship contribution statement

Irene Teixido-Orries: Writing – original draft, Visualization, Validation, Software, Methodology, Investigation, Formal analysis, Data curation, Conceptualization. **Francisco Molino:** Writing – review & editing, Writing – original draft, Supervision, Project administration, Methodology, Investigation, Data curation, Conceptualization. **Pau Agusti-Fernandez:** Visualization, Validation, Software, Methodology, Investigation, Formal analysis, Data curation. **Ebenezer Ayibiowu:** Methodology, Investigation, Conceptualization. **Derek Croucher:** Writing – review & editing, Methodology. **Angel Medina:** Supervision, Project administration, Funding acquisition. **Sonia Marín:** Writing – review & editing, Writing – original draft, Supervision, Project administration, Methodology, Funding acquisition. **Carol Verheecke-Vaessen:** Writing – review & editing, Supervision, Project administration, Methodology, Investigation, Funding acquisition, Data curation, Conceptualization.

Declaration of competing interest

The authors declare that they have no known competing financial interests or personal relationships that could have appeared to influence the work reported in this paper.

Acknowledgements

This work was supported by the Spanish Ministry of Science and Innovation (predoctoral grant FPU21/00073 and Project PID2020-114836RB-I00 funded by MCIN/AEI/10.13039/501100011033) and Cranfield University. The authors would like to thank Derek Croucher from Morning Foods for providing the contaminated oats samples for analysis.

Data availability

A DOI will be provided upon acceptance of the research paper.

References

Alisaac, E., Behmann, J., Rathgeb, A., Karlovsky, P., Dehne, H. W., & Mahlein, A. K. (2019). Assessment of *Fusarium* infection and mycotoxin contamination of wheat kernels and flour using hyperspectral imaging. *Toxins, 11*(10). https://doi.org/10.3390/toxins11100556

Badr Eldin, A. (2010). Near-infrared spectroscopy. In H. N. Pappa (Ed.), *Pharmacopeial forum, 6* p. 532). https://doi.org/10.5772/24208, 2.

Barbedo, J. G. A., Tibola, C. S., & Lima, M. I. P. (2017). Deoxynivalenol screening in wheat kernels using hyperspectral imaging. *Biosystems Engineering, 155*, 24–32. https://doi.org/10.1016/j.biosystemseng.2016.12.004

Blackshaw-Crosby, J. R. (2021). *Investigating fusarium resistance in UK winter oats*. Harper Adams University.

Brodal, G., Aamot, H. U., Almvik, M., & Hofgaard, I. S. (2020). Removal of small kernels reduces the content of *Fusarium* mycotoxins in oat grain. *Toxins, 12*, 346. https://doi.org/10.3390/toxins12050346, 2020.

De Colli, L., De Ruyck, K., Abdallah, M. F., Finnan, J., Mullins, E., Kildea, S., Spink, J., Elliott, C., & Danaher, M. (2021). Natural Co-Occurrence of multiple mycotoxins in unprocessed oats grown in Ireland with various production systems. *Toxins, 13*(3). https://doi.org/10.3390/toxins13030188

DEFRA. (2024). *Cereal and oilseed production in the United Kingdom: 2024*. Department for Environment. Food & Rural Affairs https://www.gov.uk/government/statistics/cereal-and-oilseed-rape-production/cereal-and-oilseed-production-in-the-united-kingdom-2024.

Delwiche, S. R., Kim, M. S., & Dong, Y. (2011). *Fusarium* damage assessment in wheat kernels by Vis/NIR hyperspectral imaging. *Sensing and Instrumentation for Food Quality and Safety, 5*(2), 63–71. https://doi.org/10.1007/s11694-011-9112-x

Delwiche, S. R., Rodriguez, I. T., Rausch, S. R., & Graybosch, R. A. (2019). Estimating percentages of *Fusarium*-damaged kernels in hard wheat by near-infrared hyperspectral imaging. *Journal of Cereal Science, 87*, 18–24. https://doi.org/10.1016/j.jcs.2019.02.008

Dropa, T., Dzuman, Z., & Jonatova, P. (2021). Mycotoxins in oat flakes – Changes during production and occurrence on the Czech market. *Czech Journal of Food Sciences, 39*(2), 131–139. https://doi.org/10.17221/247/2020-CJFS

European Commission. (2011). Scientific opinion on the risks for animal and public health related to the presence of T-2 and HT-2 toxin in food and feed. *EFSA Journal, 9*(12). https://doi.org/10.2903/j.efsa.2011.2481

European Commission. (2023). *Commission implementing regulation (EU) 2023/2782 of 14 December 2023 laying down the methods of sampling and analysis for the control of the levels of mycotoxins in food and repealing regulation (EC) no 401/2006*. Official Journal of the European Union.

European Commission. (2024). Commission regulation (EU) 2024/1038 of 9 April 2024 amending regulation (EU) 2023/915 as regards maximum levels of T-2 and HT-2 toxins in food. *Official Journal of the European Union L*, 1–5. https://doi.org/10.2903/j.efsa.2011.2481

Femenias, A., Gatius, F., Ramos, A. J., Sanchis, V., & Marín, S. (2020). Use of hyperspectral imaging as a tool for *Fusarium* and deoxynivalenol risk management in cereals: A review. *Food Control, 108*. https://doi.org/10.1016/j.foodcont.2019.106819

Femenias, A., Llorens-Serentill, E., Ramos, A. J., Sanchis, V., & Marín, S. (2022). Near-infrared hyperspectral imaging evaluation of *Fusarium* damage and DON in single wheat kernels. *Food Control, 142*. https://doi.org/10.1016/j.foodcont.2022.109239

Fox, G., & Manley, M. (2014). Applications of single kernel conventional and hyperspectral imaging near infrared spectroscopy in cereals. *Journal of the Science of Food and Agriculture, 94*(2), 174–179. https://doi.org/10.1002/jsfa.6367

Gil-Serna, J., Patiño, B., Verheecke-Vaessen, C., Vázquez, C., & Medina, Á. (2022). Searching for the *fusarium* spp. which are responsible for trichothecene contamination in oats using metataxonomy to compare the distribution of toxigenic species in fields from Spain and the UK. *Toxins, 14*(9). https://doi.org/10.3390/toxins14090592

Hites, R. A. (2019). Correcting for censored environmental measurements. *Environmental Science and Technology, 53*(19), 11059–11060. https://doi.org/10.1021/acs.est.9b05042

Imathiu, S. M., Ray, R. V., Back, M., Hare, M. C., & Edwards, S. G. (2017). Agronomic practices influence the infection of an oats cultivar with *Fusarium langsethiae*. *Acta Phytopathologica et Entomologica Hungarica, 52*(1), 15–28. https://doi.org/10.1556/038.52.2017.009

Isidro-Sánchez, J., D'Arcy Cusack, K., Verheecke-Vaessen, C., Kahla, A., Bekele, W., Doohan, F., Magan, N., & Medina, A. (2020). Genome-wide association mapping of *Fusarium langsethiae* infection and mycotoxin accumulation in oat (*Avena sativa* L.). *The Plant Genome, 13*(2). https://doi.org/10.1002/tpg2.20023

Janik, E., Niemcewicz, M., Podogrocki, M., Ceremuga, M., Stela, M., & Bijak, M. (2021). T-2 toxin—the most toxic trichothecene mycotoxin: Metabolism, toxicity, and decontamination strategies. *Molecules, 26*(22). https://doi.org/10.3390/molecules26226868

Krska, R., Malachova, A., Berthiller, F., & Van Egmond, H. P. (2014). Determination of T-2 and HT-2 toxins in food and feed: An update. *World Mycotoxin Journal, 7*(2), 131–142. https://doi.org/10.3920/WMJ2013.1605

Luo, S., Du, H., Kebede, H., Liu, Y., & Xing, F. (2021). Contamination status of major mycotoxins in agricultural product and food stuff in Europe. *Food Control, 127*. https://doi.org/10.1016/j.foodcont.2021.108120

Martin, C., Schöneberg, T., Vogelgsang, S., Mendes Ferreira, C. S., Morisoli, R., Bertossa, M., Bucheli, T. D., Mauch-Mani, B., & Mascher, F. (2018). Responses of oat grains to *Fusarium poae* and *F. langsethiae* infections and mycotoxin contaminations. *Toxins, 10*(1). https://doi.org/10.3390/toxins10010047

Meenu, M., Zhang, Y., Kamboj, U., Zhao, S., Cao, L., He, P., & Xu, B. (2022). Rapid determination of β-glucan content of hulled and naked oats using near infrared spectroscopy combined with chemometrics. *Foods, 11*(1). https://doi.org/10.3390/foods11010043

Rasane, P., Jha, A., Sabikhi, L., Kumar, A., & Unnikrishnan, V. S. (2015). Nutritional advantages of oats and opportunities for its processing as value added foods - A review. *Journal of Food Science and Technology, 52*(2), 662–675. https://doi.org/10.1007/s13197-013-1072-1

Schuhmacher-Wolz, U., Heine, K., & Schneider, K. (2017). Report on toxicity data on trichothecene mycotoxins HT-2 and T-2 toxins. *EFSA Supporting Publications, 7*(7). https://doi.org/10.2903/sp.efsa.2010.en-65

Serranti, S., Cesare, D., Marini, F., & Bonifazi, G. (2013). Classification of oat and groat kernels using NIR hyperspectral imaging. *Talanta, 103*, 276–284. https://doi.org/10.1016/j.talanta.2012.10.044

Su, W.-H., Yang, C., Dong, Y., Johnson, R., Page, R., Szinyei, T., Hirsch, C. D., & Steffenson, B. J. (2021). Hyperspectral imaging and improved feature variable selection for automated determination of deoxynivalenol in various genetic lines of barley kernels for resistance screening. *Food Chemistry, 343*, Article 128507. https://doi.org/10.1016/j.foodchem.2020.128507

Teixido-Orries, I., Molino, F., Castro-Criado, B., Jodkowska, M., Medina, A., Marín, S., & Verheecke-Vaessen, C. (2025). Mapping variability of mycotoxins in individual oat kernels from batch samples: Implications for sampling and food safety. *Toxins, 17*(1). https://doi.org/10.3390/toxins17010034

Teixido-Orries, I., Molino, F., Femenias, A., Ramos, A. J., & Marín, S. (2023). Quantification and classification of deoxynivalenol-contaminated oat samples by near-infrared hyperspectral imaging. *Food Chemistry*. , Article 135924. https://doi.org/10.1016/j.foodchem.2023.135924

Teixido-Orries, I., Molino, F., Gatius, F., Sanchis, V., & Marín, S. (2023). Near-infrared hyperspectral imaging as a novel approach for T-2 and HT-2 toxins estimation in oat samples. *Food Control, 153*. https://doi.org/10.1016/j.foodcont.2023.109952

Teixido-Orries, I., Molino, F., Pascari, X., Ramos, A. J., & Marín, S. (2025). Impact of processing parameters and formulation on deoxynivalenol content and transfer in oat-based beverage manufacturing. *LWT, 218*. https://doi.org/10.1016/j.lwt.2025.117368

Tekle, S., Bjørnstad, Å., Skinnes, H., Dong, Y., & Segtnan, V. H. (2013). Estimating deoxynivalenol content of ground oats using VIS-NIR spectroscopy. *Cereal Chemistry, 90*(3), 181–185. https://doi.org/10.1094/CCHEM-07-12-0084-R

Tekle, S., Mage, I., Segtnan, V. H., & Bjornstad, A. (2015). Near-infrared hyperspectral imaging of *Fusarium*-damaged oats (*Avena sativa* L.). *Cereal Chemistry, 92*(1), 73–80. https://doi.org/10.1094/CCHEM-04-14-0074-R

Thies, F., Masson, L. F., Boffetta, P., & Kris-Etherton, P. (2014). Oats and CVD risk markers: A systematic literature review. *British Journal of Nutrition, 112*, 19–30. https://doi.org/10.1017/S0007114514002281

Tittlemier, S. A., Blagden, R., Chan, J., McMillan, T. L., Pleskach, K., & Izydorczyk, M. S. (2020). Effects of processing whole oats on the analysis and fate of mycotoxins and ergosterol. *World Mycotoxin Journal, 13*(1), 45–56. https://doi.org/10.3920/WMJ2019.2530

Tittlemier, S. A., & Whitaker, T. B. (2023). Current sampling plans can introduce high variance in mycotoxin testing results as demonstrated by the online FAO Mycotoxin Sampling Tool. *World Mycotoxin Journal, 16*(2), 115–126. https://doi.org/10.3920/WMJ2022.2804

Walsh, K. B., Blasco, J., Zude-Sasse, M., & Sun, X. (2020). Visible-NIR 'point' spectroscopy in postharvest fruit and vegetable assessment: The science behind three decades of commercial use. *Postharvest Biology and Technology, 168*. https://doi.org/10.1016/j.postharvbio.2020.111246

Wan, G., Liu, G., He, J., Luo, R., Cheng, L., & Ma, C. (2020). Feature wavelength selection and model development for rapid determination of myoglobin content in nitrite-cured mutton using hyperspectral imaging. *Journal of Food Engineering, 287*. https://doi.org/10.1016/j.jfoodeng.2020.110090

Wenzl, T., Robouch, P., Schaechtele, A., Haedrich, J., Stroka, J., & European Commission. Joint Research Centre. (2016). *Guidance document on the estimation of LOD and LOQ for measurements in the field of contaminants in feed and food, EUR 28099 EN*. Luxembourg: Publications Office of the European Union.

Yan, W., Pageau, D., Martin, R., Cummiskey, A., & Blackwell, B. (2017). Is deoxynivalenol contamination a serious problem for oat in eastern Canada? *Crop Science, 57*(1), 88–98. https://doi.org/10.2135/cropsci2016.04.0263

Zareef, M., Arslan, M., Hassan, M. M., Ahmad, W., Ali, S., Li, H., Ouyang, Q., Wu, X., Hashim, M. M., & Chen, Q. (2021). Recent advances in assessing qualitative and quantitative aspects of cereals using nondestructive techniques: A review. *Trends in Food Science and Technology, 116*, 815–828. https://doi.org/10.1016/j.tifs.2021.08.012